Vol. 03, No. 01, pp. 45 –52 (2022)
ISSN: 2708-0757

JOURNAL OF APPLIED SCIENCE AND TECHNOLOGY TRENDS

www.jastt.org

Potential of Multispectral Satellite Data for Superficial Iron Oxide Detection in Sulaimaniyah, Iraqi Kurdistan Region

Ayad M. Fadhil Al-Quraishi[1*], Banaz M. Mustafa[2], P. Gopinathan[3], Y. Divya[4]

[1]*Department of Surveying and Geomatics Engineering, Tishk International University, Erbil 44001, Kurdistan Region, Iraq. ayad.alquraishi@gmail.com*

[2]*Deptartment of Soil and Water Sci., College of Agriculture, Salahaddin University, Erbil 44003, Kurdistan Region, Iraq.*

[3]*CSIR - Central Institute of Mining and Fuel Research, Ministry of Science and Technology, Govt. of India, Dhanbad, Jharkhand, 828108, India. srigopi555@gmail.com*

[4]*Department of Earth & Environment, Florida International University, Miami, FL, 33199, USA. divyayuvaraj86@gmail.com*

[*]Correspondence: ayad.alquraishi@gmail.com; ayad.alquraishi@tiu.edu.iq

Abstract

This study primarily investigates the total (Fe) iron presence in Sulaimaniyah Governorate, the Iraqi Kurdistan Region (IKR), which has an abundance of iron mines. Spatial quantification and frequent monitoring of mineral existence in the soil are essential in the mining regions. To achieve this goal, a remote sensing technique was utilized to predict soil minerals, particularly iron, in the study area using a multispectral satellite image, Landsat-7 Enhanced Thematic Mapper Plus (ETM+). A robust methodology was perceived and developed from image processing to estimate and map iron oxide-rich soils, and the soil's spectral indices were obtained after algorithms were applied in processing the bands of the Landsat image. Soil samples were collected and analyzed in the laboratory to determine the chemical, physical, and mineralogical characteristics of soils. Correlation coefficients were carried out between soil properties and spectral band values retrieved from image analysis to examine the band potentials of Landsat. The statistical results showed that there was a significant relationship between the 3rd band of the ETM+ image and each of the total iron (R^2 = 0.643), the free iron oxide (R^2 = 0.659), and sand particles (R^2 = 0.561). The predicted soil mineral maps were generated for the study area to visualize the study site's soil characterization and total iron spread. This study's results could help primarily identify the spatial distribution of some soil properties in Sulaimaniyah, Iraq.

Keywords: *Iron Oxide, Multispectral Satellite Data, Landsat ETM+, Sulaimaniyah, Iraqi Kurdistan Region.*

Received: January 15th, 2022 / Accepted: June 24th, 2022 / Online: June 30th, 2022

I. INTRODUCTION

Numerous factors govern the mineral resources of soil on Earth, and one of the main factors is iron content (Fe) [1]. Iron oxides influence the range of pH values, temperature, oxidation-reduction capacity, and water content in the soil environment. It is evidenced that Fe oxide plays a vital role in soil quality [2]. Iron (Fe) is an essential element in the Earth's crust and is the fourth most abundant element in the lithosphere after oxygen, silicate, and aluminum. It composed 5% of the Earth's crust, while its average content in soils is estimated at 3.8% [3]. Previous studies reported that the study area is rich in iron minerals; even the small proportion in specific soil has iron content. In Mosul governorate, Iraq, the total Fe concentration in five soil samples ranged from 3.45 to 4.89 % [4]. The total Fe concentration ranged between 4.5 to 6.6 % in four Erbil calcareous soils [5]. Meanwhile, the total Fe content of the soil from Abu-Gharib is 3.42 % [6]. The total Fe concentration ranged between 1.39 to 6.45 % in some alluvial fan soils [7]. Al-Jadoa [8] reported that Fe's total concentration is ranged between 1.7 and 3.85 % in the soil samples taken from sedimentary plain, undulatory, and Jazeera region. Examining a group of soils at Aski Kalak soil showed that the total Fe concentration ranged from 0.54 to 2.13 % [9]. The Hussainiyat ironstone deposit, where the mines are in, contains mainly goethite and haematite [10]. Sposito [11] reported Fe oxides' intense pigments to give many soils their red, yellow, orange, or brown color even at low concentrations (fewer percent). Prior studies depicted that the study area region has a good source of iron minerals in soils, and

doi: 10.38094/jastt301171

it needed any non-destructive technique for quantifying the iron oxide.

Identifying and retrieving the number of iron minerals from the soil is a challenging task, and there is an advanced technology required to achieve it. After investigating the previous works involved in soil minerals studies, remote sensing/geoinformatics technology was used for its potential and rapid mapping. The visible -near-infrared (NIR) region of spectroscopy is used in many studies for analyzing soil properties. The color of soil indirectly represents few Soil properties such as organic matter, carbonates, and iron oxides [12]. Hence, the spectroscopy's visible range can be used to get detailed soil color data [2]. Iron ions can easily substitute into octahedral sites and less into tetrahedral sites, thus retained in soils. This can majorly affect spectroscopy absorption features [13, 14]. Remote sensing datasets and techniques were effectively used in several environmental applications in several countries [15-23]. The surface mineralogical features can be effectively mapping by remote sensing technology, especially Iron oxide, which has significant influences on the soil's spectral reflectance characteristics [24]. Al-Quraishi, et al. [18] has utilized a Landsat ETM+ image, soil chemical and physical properties laboratory analyses, and statistical analysis to find the statistical correlations among the physicochemical and spectral properties of soil in some sites of the IKR.

The soil index map is different from that of the ferrous minerals in such a way that the iron oxide includes all the materials showing red color on the ground. In other words, it includes iron ores, red soils, and laterites [25]. The mineral-specific color results from their interaction with visible light and depends on both the crystal structure and particle size but several studies using the NIR region for getting effective results in the analysis of iron oxide. Utilizing satellite images has potentially given more significant correlations to the field data in iron oxide analysis, specifically Landsat images [26-31]. The freely available Landsat data used in this study experiment with the Iron oxide existence in the IKR soils in northern Iraq. This region possibly exploits local iron oars and represents iron mines in the Bawari Valley [32].

Along with multispectral data, GIS tools enhanced this study by mapping soil properties. GIS manipulated the soil properties as attributes and helped visualize the study site's soil classification [33-36]. The current study's main objectives are: 1) To examine the potential of geoinformatics techniques to depict, map, and assess the iron-rich soils in the study region using the Landsat -7 ETM+ image, 2) To process the ETM+ image and retrieve band details and other spectral indices for soil analysis, 3) To generate a statistical regression model between the spectral indices retrieved from satellite image and soil lab data and test the predicted models' significance.

II. Study Area

The study area for this research (Fig. 1) is a part of the Sulaimaniyah Governorate in the IKR (North of Iraq), which covers an area of (9,829.0) Km^2. The IKR majorly has a combination of flatlands, hills, valleys, and mountains. The study area's main features are located between Qandil, Sara, Peramagron, Sagrma, Swren, Mlakawa, and Goezha mountains, which reach in height up to 3,600 m above sea level (a.s.l.) with snow coverage at high altitudes. A smoother morphology occurs in the central part. However, the high area is characterized by an anticline or syncline system [37], which gives rise to relief with a general orientation NE-SE. The study area's climate shows typical Mediterranean environments' typical characteristics [38, 39].

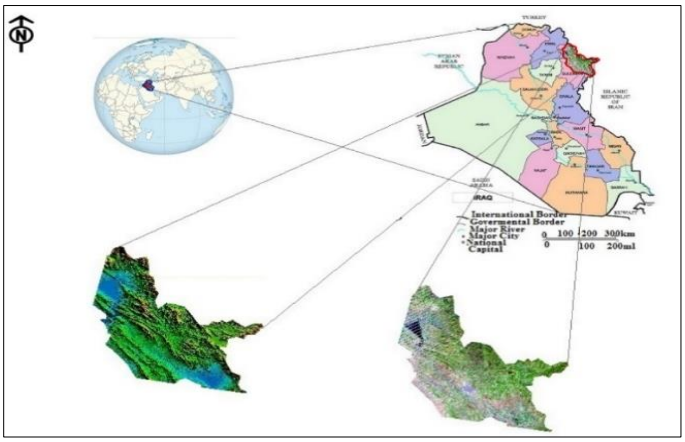

Fig. 1. Location map of the study area with its Landsat7 ETM+ RGB 741color composite and the DEM.

The Sulaimaniyah Governorate comprises twelve districts, which are: Sulaimaniyah, Halabja, Derbandikhan, Kalar, Chamchamal, Chwarta, Penjuin, Dukan, Qaladza, Qaradagh, Shahrazoor, and Rania. Sulaimaniyah city is located 400km North-East of Baghdad, the capital city of Iraq. The study site was divided into three zones with 39 sampling locations for further soil chemical and physical laboratory analyses, as shown in Fig. 2.

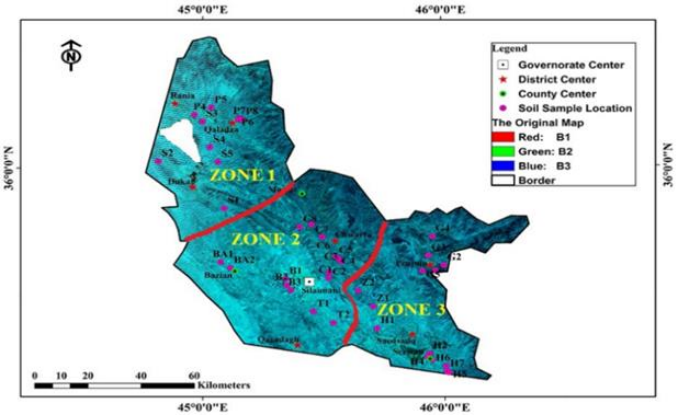

Fig. 2. The three zones of the study area.

III. Materials and Methods

A. Collection and Preparation of Soil Samples

The current study methodology is divided majorly into three parts (Field, Laboratory, and Office) that are described in the flowchart in Fig 3. Thirty-nine soil samples were collected from different Sulaimaniyah Governorate locations from July 2012 to June 2013 (Fig. 2). The samples were taken from the soil surface

layer (0-15) cm depth. After passing the soil samples through a 2 mm sieve series (ASTM). The sieved soil samples are taken to determine the physical, chemical, and spectral characteristics properties. Similarly, the soil samples passed through (0.425) mm sieve for determining the Percent Linear Shrinkage (PLS) test. The study areas had different soil colors indicated by using Munsell color parameters (Hue, Value, and Chroma) observable in the field. For each soil sample (dry and moist) the color was among the followings: (Brown, Dark Brown, Very Dark Brown, Strong Brown, Dark Grayish Brown, Very Dark Grayish Brown, Yellowish Brown, Light Yellowish Brown, Dark Yellowish Brown, Pole Brown, Dark Reddish Brown, Olive Brown, Light Olive Brown, and Pink). The sample collection was completed one by one zone, as shown in Fig.2.

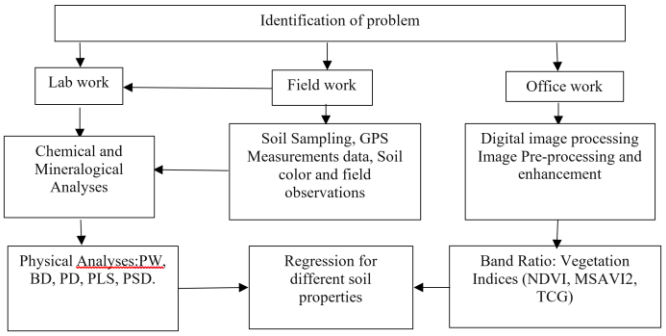

Fig. 3. Methodology flowchart

B. Soil Laboratory Analyses

The following physical analyses are done to obtain the soil physical and chemical properties for the study's soil samples: Particle size distribution was performed by the pipette method [40]. Bulk density is determined using the clod method covering the samples with paraffin wax, as described by Black, 1965. Specific gravity (using pycnometer) particle density and liquid limit tests were determined as per ASTM [41] guidelines. The percent of linear shrinkage was measured according to the British Standards Institution method, 1975. Soil moisture content was measured by the gravimetric method, as mentioned in Gardner [42].

The chemical analyses were conducted on soil extract 1:2 (Soil: H_2O) as explained in the following sentences. The electrical conductivity was measured using an EC- meter. The soil's pHwas measured using a pH-meter model described in prior works [40]. Sodium and potassium ions were determined by the flame photometer method model. Organic matter (OM) was measured by the Walkley and Black method [43]. Calcium carbonate was determined by the acid neutralization method, according to Rowell [44]. Cation exchange capacity was determined to utilize (1N) NaOAC solution (pH = 8.2), and Available phosphorus was measured by using the Olsen procedure in Ryan, et al. [45]. Total nitrogen was estimated by the Kjeldahl digestion-distillation method in Bremner and Mulvaney [46]. The soluble cations and anions were determined according to the procedures outlined in Bremner [47]. The total iron was digested by the Kjeldahl method as reported in [46] and then measured by an Atomic absorption spectrometer (AA 700) with a wavelength (248.3nm). Iron oxide removal from soils and clays by a dithionite- citrate system buffered with sodium bicarbonate and measured by an Atomic absorption spectrometer [48]. Table I shows the different soil properties of the study area according to its sampling points. The soil properties indicated that there is a wide range of iron oxide existence. The pH, EC, and OM values of soils are shown to encouraging crop growth conditions.

C. Landsat Dataset and Image Processing

A Landsat 7 ETM+ (path 168/row 35) acquired on (1st Sep 2012) was downloaded for the study region with a 30m spatial resolution. The Landsat ETM+ imagery was radiometrically corrected to eliminate the cls-off error using a histogram matching technique in ENVI 5.3. The seven bands pixel values were retrieved for each sampling site after the image processing. The freely available data and most successful geosciences studies promoting Landsat satellite data are necessary for remote sensing analysis. Prior studies evidenced that Red and NIR regions were best suited for iron mapping [49]. SWIR and NIR regions eased to identify soil classification. Landsat ETM+ image was geometrically corrected in datum WGS84 and projection UTM zone N38 using first order (linear) of a polynomial function and Nearest Neighbor rectification re-sampling, which was chosen to preserve the radiometry and spectral information in the imagery. The Landsat image was radiometric calibrated and converted into reflectance at sensor values using the ENVI software.

IV. Results and Discussion

A. Spatial Analysis

In a raster model, the spatial analysis would refer to patterns and covariations in pixel values of one or more data layers. Topics include network analysis, point pattern analysis, trend analysis, spatial interpolation, sampling, and exploratory data analysis [33]. Modeling requires a good understanding of the system being modeled, and it incorporates several steps [50]. After the necessary transformations, we investigated possible relationships between soil chemical and physical properties and the Landsat ETM+ image-based DN values of the soil samples's location by correlation (Pearson) analysis and then modeling the significant linear regression relationships. This analysis considered only the strong and significant (positive or negative correlations) relationships for developing robust models [51].

Modeling the relationships between Landsat-7 ETM+ bands DN values with soil surface variables enabled to map of these soil variables on a spatially explicit basis. The soil variables selected for linear regression analysis show the most substantial positive or negative correlations with the ETM+ bands' DN values. Dogan and Kilic [51] indicated that the modeling is the relationship between Landsat-7 ETM+ bands DN values and some soil surface variables enabled us to map these soil variables on a spatially explicit basis.

The produced soil properties models were converted to grid map layers by utilizing the correlated Landsat-7 ETM+ bands and the ERDAS ERMapper package. The outcomes of simple linear regression were summarized in models.

TABLE I. THE CHEMICAL AND PHYSICAL PROPERTIES OF THE STUDY AREA SOIL SAMPLES

Sample ID	Zone	Sample Locations	EC	PH	OM	PSD sand gm/kg	Total Fe	Free Iron Oxide	Free Fe / Total Fe
H1	Zone 3	KaniPanka	0.25	7.26	15.3	32.5	4.63	2.97	0.64
H2	Zone 3	Serwan1	0.22	7.1	11.9	33.0	3.10	1.9	0.61
H3	Zone 3	Serwan2	0.20	7.2	21.3	81.2	2.30	2.12	0.92
H4	Zone 3	Kelaspe	0.20	7.25	21.3	59.1	4.93	3.62	0.73
H5	Zone 3	QlejiAnab	0.25	7.19	23.2	89.8	3.10	0.34	0.1
H6	Zone 3	Darashesh	0.20	7.76	22.0	147.4	1.89	0.32	0.16
H7	Zone 3	Anab	0.21	7.95	19.9	71.5	2.06	0.22	0.1
P4	Zone 1	Rania	0.20	7.83	10.9	69.0	5.10	1.32	0.25
P5	Zone 1	Bastasen	0.20	7.88	10.6	70.3	6.40	1.63	0.25
P6	Zone 1	Qaladza	0.25	7.84	15.3	164.4	7.28	1.84	0.25
P7	Zone 1	QutkeHasar	0.25	7.83	15.3	180.7	7.91	1.45	0.18
P8	Zone 1	Dere	0.35	7.74	19.9	332.0	49.40	16.65	0.33
C1	Zone 2	Sharisten	0.19	7.27	32.0	112.3	5.14	2.02	0.39
C2	Zone 2	Bnawela	0.20	7.20	27.9	133.6	15.57	3.22	0.2
C3	Zone 2	Kani Sard1	0.19	7.19	15.3	55.0	16.81	16.6	0.98
C4	Zone 2	Kani Sard2	0.30	7.20	8.6	153.8	25.44	17.26	0.67
C5	Zone 2	Kani Sard3	0.20	7.27	3.3	400.7	28.18	18	0.63
C6	Zone 2	Wazha	0.20	7.17	15.3	194.0	31.09	15.45	0.49
C7	Zone 2	Kunamase	0.22	7.25	4.5	88.8	21.64	16.26	0.75
C8	Zone 2	Kareza	0.21	7.20	21.3	33.5	22.77	15.57	0.68
B1	Zone 2	ZankoeAmreke	0.21	7.17	15.9	41.5	9.14	2.01	0.21
B2	Zone 2	Twezhenawa	0.32	7.89	15.9	51.6	5.35	2.03	0.37
B3	Zone 2	Bakrajo	0.25	7.92	19.9	87.0	8.34	1.65	0.19
S1	Zone 1	Surdash	0.20	7.28	18.6	80.7	3.67	1.49	0.4
S2	Zone 1	KaniMazu	0.20	7.37	23.3	69.5	3.47	1.74	0.5
S3	Zone 1	BardaKoz	0.21	7.37	11.9	47.0	6.80	2.09	0.3
S4	Zone 1	Sewkan	0.22	7.27	13.3	59.4	5.56	1.63	0.29
S5	Zone 1	Kunamar	0.29	7.32	11.9	65.0	2.66	2.27	0.85
BA1	Zone 2	Baziyan1	0.25	7.01	17.3	99.9	3.40	1.11	0.32
BA2	Zone 2	Baziyan2	0.40	7.97	17.3	73.3	2.81	2.17	0.77
T1	Zone 2	Zrguez	0.29	7.05	11.9	92.5	3.34	1.62	0.48
T2	Zone 2	Tanjaro	0.30	7.92	20.6	232.8	13.74	1.48	0.1
Z1	Zone 3	Barzinja	0.20	7.00	11.9	18.5	3.45	1.13	0.32
Z2	Zone 3	Gelara	0.20	7.19	21.3	23.0	4.17	3.17	0.76
G1	Zone 3	Blekyan	0.16	7.19	37.2	457	21.62	15.75	0.72
G2	Zone 3	Bashmax	0.27	7.20	65.2	272	19.12	12.15	0.63
G3	Zone 3	Kelw	0.18	7.17	18.6	489	24.42	17.84	0.73
G4	Zone 3	Garmk	0.21	7.37	15.3	66.0	17.91	2.05	0.11
G5	Zone 3	Penjuin	0.17	7.46	9.9	152.0	19.23	2.34	0.12

The model summary reported the correlation coefficient (r) between the dependent variable's observed and predicted values. The regression model explained the coefficient of determination (R^2) in the dependent variable. The produced [Free Fe, Total Fe, and Sand] maps from the developed models had two main advantages. First, they established an updated spatial database of the focused soil variables. Second, they presented a chance for monitoring processes that could reveal temporal changes. The model was then used to predict the full extent of the original map. Moreover, the regression statistics showed that the developed models were robust.

B. Statistical Correlations

Pearson correlation coefficients of the raw data were calculated with their significance values. The correlation was simply the covariance measured for standardized variables. To standardize a variable mean value was subtracted from all measurements, and the result was divided by the standard deviation [33]. The regression models were demonstrated for all the tested soil properties with the entire spectral bands of Landsat, but here the best-suited variables are only presented for further discussion. The model summary that the regression model explained the correlation coefficient (r) between the observed and predicted values of the dependent variable and the coefficient of determination (R^2) in the dependent variable. Large values (close to 1) of (r) and R^2 indicated a strong relationship and well-fitted model, respectively, using the SPSS package. Experimental models are essential tools for relating field-measured variables remotely sensed data. The regression analysis has been a prevalent empirical method of linking these two types of data to supply continuous environmental variables estimates [52]. Then defined soil chemical and physical properties and ETM+ bands' DN values as dependent (y) and independent (x) variables. Prediction models mapping for regression showed 15 strong (positive and negative correlations) relationships for developing robust models. Consequently, 15 sets of linear regression were employed to develop eight distinct models shown in Table II. Each model is classified into five classes that were very low, low, moderate, high, and very high. Means, minimums, maximums, medians, skewness, and coefficient of variations (CVs) of selected soil properties were calculated using statistical software. Data normality was tested using the Anderson-Darling (A-D) test using statistical software at a significance level of 5%. Pearson correlation coefficients were calculated for all soil properties and data [53].

Numerous soil properties governed the spectral bands. For example, Bowers and Hanks [54] indicated that with increasing particle size from 2200 to 2650 nm, at least an additional 14.6 % of the direct solar radiant energy was found to be absorbed. From Table I, it can be inferred that the particle size of sand influenced the 3rd ETM+ band region with reasonable accuracy (R^2=0.561). West, et al. [55] supported this view by explicating particle size's influence on soil spectral reflectance revealed rapid in 485 nm. Theoretically, a decrease in the particle size would increase reflectance. This increment is caused by heavier light scattering and lower extinction of light, passing through the particles [56]. Fine textures generally show greater reflectance than coarse textures [57]. Besides particle size, soil spectral reflectance is also affected by other particle characteristics, such as sphericity and micro-roughness at the surface of textural elements [58]. This study found that the 3rd band of the ETM+ image is the best band suited for sand particle modeling.

TABLE II. SUMMARY OF LINEAR REGRESSIONS EQUATIONS FOR DIFFERENT MODELS UTILIZING THE ETM+ IMAGE BANDS

Model	**R^2**	**Regression Equation**
Free Iron Oxide & Band 3	0.659	Free Fe_2O_3 = 45.137 + (-180.290) (B3)
Total Fe & Band 3	0.643	Total Fe = 62.897 + (-235.390) (B3)
Sand & Band 3	0.561	Sand = 822.751 + (-3309.011) (B3)
Total N & Band 1	0.277	N = 3.676 + (-12.802) (B1)
Na_2O & Band 7	0.262	Na_2O = 0.676 + (- 2.207) (B7)
O.M& Band 6	0.207	O.M = 607.727 + (-1.864) (B6)
K & Band 1	0.205	K = 0.853 + (-4.976) (B1)
Mg & Band 2	0.204	Mg = 1.315 + (- 4.455) (B2)

The total iron and free iron oxide governed well in the 3rd ETM+ band region as well. It has shown a strong correlation with the highest correlation values (R^2=0.659) and (R^2=0.643), respectively. Dematte, et al. [49] found many of the absorption features in soil reflectance spectra are due to the presence of iron in some form. The main absorption bands were centered at 450 and 850nm and were attributed to interactions between EMR and iron oxide content in the soil. One of the earliest studies by Obukhov and Orlov [59] researched that decreases in reflectance with increasing iron oxide percentage in the visible region of the spectrum (500-640 nm). The results revealed a negative significant between the 6th band of ETM+ and OM by (R^2 = 0.207), which means the temperature decreased when the OM content increased.

In the regression analyses, soil variables were defined as dependent (y) variables, while the Landsat-7 ETM+ bands DN variables were considered independent (x) variables. The obtained models were then explained using equations for the form y = a + bx formula [51].

The validation test was carried out to check the regression models to represent the estimated soil properties' spatial existence for total iron and free iron oxide compared to laboratory analyses. The results showed that the predicted and measured results define nature's reality. The regression-based predicted maps are shown in Figs. 4, 5, 6. Similarly, other locations such as (C4, C6, C7, C8, G1, and G3) that recorded a high value of total Fe are indicated by orange color in Fig. 4. On the other side, regression model maps (Figs. 4,5) were the very high class pointed by the blue color of total Fe and free iron oxide, at the east of the study area was very high. While the iron oxide was (Fig. 4), the very high class was the brown color in most study areas. The sample validations had the same reality as the results of the laboratory analyses and spectral prediction models. Predictive performances of the fitted models are checked based on cross-validation.

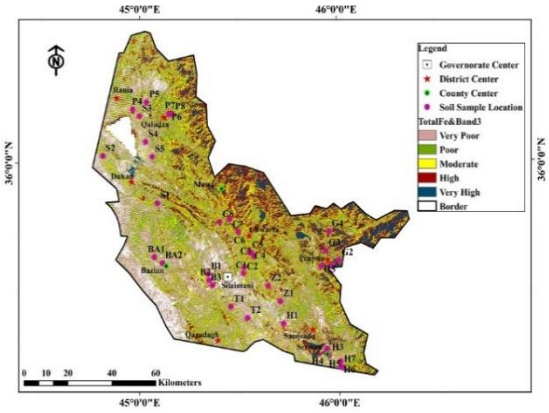

Fig. 4. The regression-based classified map of the (Total Fe) using the third band of the ETM+

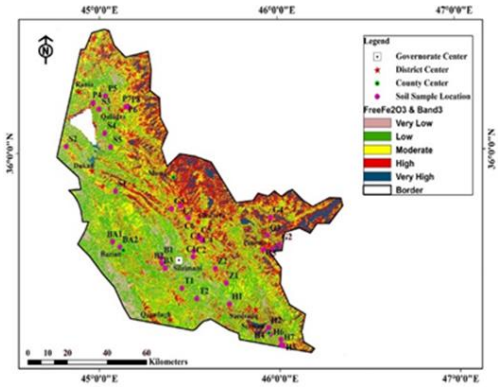

Fig. 5. The regression-based classified map of (free Fe2O3) using the third band of the ETM+

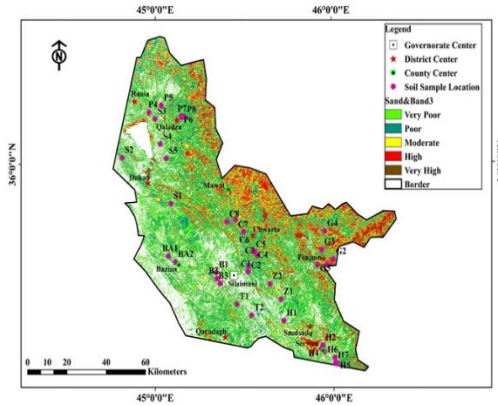

Fig. 6. The regression-based classified map of sand particles using the third band of the ETM+

V. CONCLUSIONS

According to the results of the present study, the following conclusions were extracted:

- Modeling the specific soil minerals and spatial distribution using DN numbers of Landsat image is thinkable with reasonable accuracy.
- The Landsat-7 ETM+ image bands' statistical analyses revealed a significant negative correlation ($R^2 = 0.659$) between the free iron and band 3 (Red). When the amount of free iron in soil increased, the reflectance decreased, similarly with the total iron ($R^2 = 0.643$) and band3 (Red). High iron content contributed to the lower reflectance.
- This study predicted an interesting fact about soil sand particles dominance in the third band of the Landsat 7 ETM+ image along with iron content of soils evidenced with good correlation (R^2=0.561). This will lead to further future soil textural analysis.
- The current study evidenced that geoinformatics techniques can be utilized for iron mineral quantification and non-destructive methods. This study results can be used at the agriculture research stations to improve the agricultural conditions in IKR.

ACKNOWLEDGMENT

The authors would like to thank and extend their gratitude to the United States Geological Services (USGS) for the free available Landsat satellite images.

REFERENCES

[1] J. W. Stucki, B. A. Goodman, and Schwertmann, *Iron in Soils and Clay Minerals* (NATO Science Series C: 1988). Springer, 1988.

[2] R. A. Rossel, E. N. Bui, P. Caritat, and N. J. McKenzie, "Mapping iron oxides and the color of Australian soil using visible‐nea r ‐ infrared reflectance spectra," *J. Geophys. Res.*, vol. 115, p. F04031, 2010 2010, doi: 10.1029/2009JF001645.

[3] W. L. Lindsay, *Chemical equilibria in soils*. Wiley Inter science, 1979.

[4] Z. Al-Aathami, "Studies of some effecting factors in iron availability in alluvial and brown soil [in Iraq]," 1981.

[5] S. D. Al-Malak, "Iron availability in some calcareous soils in northern Iraq," M.Sc. thesis, Salahadin University, Erbil, 1986.

[6] K. M. N. Al-Azawy, "Influence of nitrogen and iron application on growth, yield and nutrie nt content of soil and corn plant," M.Sc. Thesis, Baghdad Univ., 1988.

[7] I. J. Mohamed, "The chemical behavior of zinc, copper, and other selected nutrients el ements in some Iraqi arid soils," Ph. Degree Thesis, State Univ. of Ghent, 1988.

[8] A. K. Al-Jadoa, "Iron, manganese, zinc, and copper in soil particles," Ph.D. Thesis, Baghdad Univ., 1990.

[9] M. A. J. Al-Obaidi, N. F. Khalil, and M. Sadullah, "Iron status in some soils of Northern Iraq," *Jour. Agron. Sci.*, no. 2, 1994 1994.

[10] K. S. Al-Bassam and M. Y. Tamar-Agha, "Genesis of the Hussainiyat ironstone deposit, Western Desert, Iraq," *Mineralium Deposita*, vol. 33, pp. 266-282, 1998 1998.

[11] G. Sposito, *The Chemistry of Soils*. Oxford University Press, 1989.

[12] M. F. Baumgardner, L. F. Silva, L. L. Biehl, and E. R. Stoner, "Reflectance properties of soils," *Advances in Agronomy*, vol. 38, pp. 1-44, 1985 1985.

[13] G. R. Hunt, B. S. Siegal and A. R. Gillespite, Eds. *Electromagnetic radiation: The communications link in remote sensing*. Wiley, 1980.

[14] R. A. Weismiller, V. S. G. E, P. S. E, L. K, and B. M.F, "Use of soil spectral properties for monitoring soil erosion," *Proc. Conf. Soil Erosion and Conservation*, pp. 119-127, 1985 1985.

[15] A. M. Fadhil, "Drought mapping using Geoinformation technology for some sites in the Iraqi Kurdistan region," *Int. Journal of Digital Earth*, vol. 4, no. 3, pp. 239-257, 2011 2011, doi: 10.1080/17538947.2010.489971.

[16] A. M. Fadhil, "Sand dunes monitoring using remote sensing and GIS techniques for some sites in Iraq," 2013, 2013///, doi: 10.1117/12.2019735.

[17] W. Wu, A. S. Muhaimeed, W. M. Al-Shafie, and A. M. F. Al-Quraishi, "Using L-band radar data for soil salinity mapping—a case study in Cent ral Iraq," *Environ. Res. Commun.*, vol. 1081004, 2019 2019, doi: 10.1088/2515-7620/ab37f0.

[18] A. M. F. Al-Quraishi, H. A. Sadiq, and J. P. Messina, "Characterization and Modeling Surface Soil Physicochemical Properties Using Landsat Images: A Case Study in the Iraqi Kurdistan Region," 2019, vol. XLII-2/W16, 2019///, pp. 21-28, doi: 10.5194/isprs-archives-XLII-2-W16-21-2019.

[19] A. S. Alqasemi, M. E. Hereher, G. Kapland, A. M. F. Al-Quraishi, and H. Saibi, "Impact of COVID-19 lockdown upon the air quality and surface urban hea t island intensity over the United Arab Emirates," *Science of The Total Environment*, vol. 767, p. 144330, 2021 2021, doi: 10.1016/j.scitotenv.2020.144330.

[20] M. Kumar, A. M. F. Al-Quraishi, and I. Mondal, "Glacier changes monitoring in Bhutan High Himalaya using remote sensin g technology," *Environmental Engineering Research*, vol. 26, no. 1, p. 190255, 2021 2021, doi: 10.4491/eer.2019.255.

[21] A. M. F. Al-Quraishi, H. A. A. Gaznayee, and M. Crespi, "Drought Trend Analysis in Sulaimaniyah (Iraqi Kurdistan Region) for th e Period 1998-2017 using Remote Sensing and GIS," *J. of Arid Land*, 2021 2021.

[22] W. Wu *et al.*, "Soil salinity prediction and mapping by machine learning regression in Central Mesopotamia, Iraq," *Land Degradation and Development*, vol. 29, no. 11, pp. 4005-4014, 2018 2018, doi: 10.1002/ldr.3148.

[23] Y. Yao *et al.*, "Evaluation of EDI derived from the exponential evapotranspiration mode l for monitoring China's surface drought," *Environmental Earth Sciences*, vol. 63, no. 2, pp. 425-436, 2011 2011, doi: 10.1007/s12665-011-0972-5.

[24] A. Ciampalini, F. Garfagnoli, and B. Antonielli, "Remote sensing techniques using Landsat ETM+ applied to the detection of iron ore deposits in Western Africa," *Arab J Geosci*, vol. 6, pp. 4529-4546, 2013 2013, doi: 10.1007/s12517-012-0725-0.

[25] P. Gopinathan, S. Parthiban, T. Magendran, A. M. F. Al-Quraishi, A. K. Singh, and P. K. Singh, "Mapping of ferric (Fe3+) and ferrous (Fe2+) iron oxides distribution u sing band ratio techniques with ASTER data and geochemistry of Kanjama lai and Godumalai, Tamil Nadu, south India," *Remote Sensing Applications: Society and Environment*, vol. 18, p. 100306, 2020 2020, doi: 10.1016/j.rsase.2020.100306.

[26] D. F. Ducart, A. M. Silva, C. Labouré, B. Toledo, and L. M. Assis, "Mapping iron oxides with Landsat-8/OLI and EO-1/Hyperion imagery from the Serra Norte iron deposits in the Carajás Mineral Province, Brazil," *Brazilian Journal of Geology*, vol. 46, no. 3, 2016 2016.

[27] A. A. Madani, "Utilization of Landsat ETM+ Data for Mapping Gossans and Iron Rich Zon es Exposed at Bahrah Area, Western Arabian Shield, Saudi Arabia," *Earth Sci.*, vol. 20, no. 1, pp. 35-49, 2009 2009.

[28] K. White, J. Walden, N. Drake, F. Eckardt, and E. Settlell, "Mapping the iron oxide content of dune sands, Namib Sand Sea, Namibia, using landsat thematic mapper data," *Remote Sensing of Environment*, vol. 62, no. 1, pp. 30-39, 1997 1997.

[29] R. T. Mzuri, A. A. Omar, and Y. T. Mustafa, "Spatiotemporal analysis of vegetation cover and its response to terrain and climate factors in Duhok Governorate, Kurdistan Region, Iraq," *The Iraqi Geological Journal*, pp. 110-126, 2021.

[30] Z. Adil, S. Jabbar, R. H. Sulaiman, Y. T. Mustafa, and H. Karimi, "Land suitability analysis for identifying industrial zones in Duhok District, Kurdistan Region of Iraq," *Journal of Civil Engineering Frontiers*, vol. 2, no. 02, pp. 51-56, 2021.

[31] Y. T. Mustafa, "Multi-temporal Satellite Data for Land Use/Cover (LULC) Change Detection in Zakho, Kurdistan Region-Iraq," in *Environmental Remote Sensing and GIS in Iraq*: Springer Water, 2020.

[32] P. R. S. Moorey, *Ancient Mesopotamian Materials and Industries*. Oxford University Press, 1994.

[33] P. M. Mather and M. Koch, *Computer Processing of Remotely-Sensed Images*, Fourth Edition ed. John Wiley, 2011.

[34] Y. Divya, P. Gopinathan, K. Jayachandran, and A. M. F. Al-Quraishi, "Color slices analysis of land use changes due to urbanization in a cit y environment of Miami Area, South Florida, USA," *Model. Earth Syst. Environ.*, 2020 2020, doi: 10.1007/s40808-020-00883-x.

[35] Y. Mustafa, "Spatiotemporal Analysis of Vegetation Cover in Kurdistan Region-Iraq using MODIS Image Data," *Journal of Applied Science and Technology Trends*, vol. 1, no. 1, pp. 01-07, 03/10 2020, doi: 10.38094/jastt119.

[36] S. Zakaria, N. Al-Ansari, Y. Mustafa, M. Alshibli, and S. Knutsson, "Macro rain water harvesting network to estimate annual runoff at Koysinjaq (Koya) district, Kurdistan region of Iraq," *Engineering*, vol. 5, no. 12, pp. 956-966, 2013.

[37] M. Boccaletti and P. Dainelli, *RegmaticosystemNeogenico-Quaternary Mediterranean nell'area: esempio d i deformazione plastic-collisionale rigid post*. Memorial Society of Geology, 1982.

[38] C. Buondonno, A. P. Leone, F. Ortolani, S. Pagliuca, and P. Tedeschi, *Marginal area 'Fortorebeneventano'. Help diattito excursion*. National Council of Research Department: Irrigation Institute, 1987.

[39] A. P. Leone, G. G. Wright, and C. Corves, "The application of satellite remote sensing for soil studies in upland areas of Southern Italy," *NT. J. Remote Sensing*, vol. 16, no. 6, pp. 1087-1105, 1995 1995.

[40] L. R. Van Reeuwijk, *Procedures for soil analysis*, 5th edition ed. (Technical paper 9). International soil reference, 1995.

[41] ASTM, *Standard test methods for liquid limit, plastic limit, and plasticity index of soils*. ASTM International, 1986.

[42] W. H. Gardner, "Water content," *Methods of soil Analysis*, pp. 493-544, 1986 1986.

[43] D. W. Nelson and L. E. Sommers, "Total carbon, organic carbon, and organic matter," *Methods of soil analysis. Part 2. Chemical and microbiological propert ies*, pp. 539-580, 1982 1982.

[44] D. L. Rowell, *Soil science: Methods and applications*. Longman. Group UK Limited, 1996.

[45] J. Ryan, G. Estefan, and A. Rashid, *Soil and plant analysis laboratory manual*, 2nd edition ed. International Center for Agriculture Research in the Dry Areas (ICARDA), 2001.

[46] J. M. Bremner and C. S. Mulvaney, "Nitrogen - Total," *Methods of soil analysis. Part 2. chemical and microbiological propert ies*, pp. 595-622, 1982 1982.

[47] J. M. M. Bremner, C. S. , A. L. Page and others, Eds. *Methods of soil analysis. Part 2. Chemical and microbiological propert ies* (Agron. Monogr. 9). ASA, 1982.

[48] O. P. Mehra and M. L. Jackson, "Iron oxide removal from soils and Clays by a dithionite- citrate syste m buffered with sodium bicarbonate," *Madison, Wisconsin*, 1955 1955.

[49] J. A. M. Dematte, M. R. Nanni, A. R. Formaggio, and J. C. N. Epiphanio, "Spectral reflectance for the mineralogical evaluation of Brazilian low clay activity soils," Ph.D. Thesis, Sao Paulo, Brazil, 2006.

[50] M. J. Barnsley, *Environmental Modeling: A Practical Introduction*. CRC Press, 2007.

[51] H. M. Dogan and O. M. Kilic, "Modeling and mapping some soil Surface properties of Central Kelkit Ba sin in Turkey by using Landsat-7 ETM+ images," *Int. J. of Remote Sensing*, vol. 3, no. 15, pp. 5623-5640, 2013 2013.

[52] W. B. Cohen and S. N. Goward, "Landsat's Role in Ecological Applications of Remote Sensing," *Bioscience*, vol. 54, pp. 535-545, 2004 2004.

[53] F. S. Khan, Q. U. Zaman, A. A. Farooque, and S. R. Saleem, "Relationship of soil properties to apparent ground conductivity in wil d blueberry fields," *Truro, Nova Scotia, Canada*, 2012 2012.

[54] S. A. Bowers and R. J. Hanks, "REFLECTION OF RADIANT ENERGY FROM SOILS," *Soil Science*, vol. 100, no. 2, 1965. [Online]. Available: https://journals.lww.com/soilsci/fulltext/1965/08000/reflection_of_radiant_energy_from_soils.9.aspx.

[55] S. L. West, G. N. White, Y. Deng, K. J. McInnes, and J. B. Dixon, "Kaolinite, halloyside, and iron oxide influence on physical behavior o f formulated soils," *Soil Science Society of America Journal*, vol. 68, pp. 1452-1460, 2004 2004.

[56] NASA, *Ada style guide* (no. SEL-87-002). NASA, Goddard Space Flight Center, 1987.

[57] E. H. Horvath, D. F. Post, and J. B. Kelsey, "The relationships of Landsat digital data to the properties of Arizona Rangeland," *Soil Science Society American Journal*, vol. 48, pp. 1331-1334, 1984 1984.

[58] M. A. Mulders, *Remote sensing in soil science* (Developments in soil science). Elsevier, 1987.

[59] A. I. Obukhov and D. S. Orlov, "Spectral reflectivity of the major soil groups and possibility of usin g diffuse reflection in soil investigations," *Soviet Soil Science (Engl. Transl)*, vol. 2, pp. 174-184, 1964 1964.